Electrochimica Acta 201 (2016) 30–37

Contents lists available at ScienceDirect

Electrochimica Acta

journal homepage: www.elsevier.com/locate/electacta

Comparison of Two-Dimensional Transition Metal Dichalcogenides for Electrochemical Supercapacitors

Mark A. Bissett[a,*], Stephen D. Worrall[a], Ian A. Kinloch[b], Robert A.W. Dryfe[a,*]

[a] School of Chemistry, University of Manchester, Oxford Road M13 9PL, United Kingdom
[b] School of Materials, University of Manchester, Oxford Road M13 9PL, United Kingdom

ARTICLE INFO

Article history:
Received 30 October 2015
Received in revised form 30 March 2016
Accepted 30 March 2016
Available online 31 March 2016

Keywords:
Supercapacitor
pseudocapacitor
transition metal chalcogenide
energy storage
coin cell

ABSTRACT

Layered two-dimensional (2D) materials such as transition metal dichalcogenides (TMDCs) are receiving increased interest for applications in energy storage due to their high specific surface area and versatile electronic structure. In this work, we prepare solvent stabilised dispersions of a variety of few-layer thick TMDC crystals (MoS_2, $MoSe_2$, WS_2, and TiS_2) by ultrasonication. The exfoliated materials were first characterised by a variety of techniques to determine their quality. These dispersions were then used to form supercapacitor electrodes by filtration, without use of any further conductive additives or polymeric binders. These thin layer TMDC electrodes were assembled into symmetrical coin-cell devices for comparative electrochemical testing. It was found that despite being the most widely studied material, MoS_2 suffers from inferior charge storage properties compared to the much higher conductivity and lower density TiS_2. Impedance spectroscopy was used to investigate the charge storage mechanisms inside the coin cells, which were found to consist of a combination of both rapid, but low magnitude, electric double layer capacitance and much slower, but higher magnitude, ion adsorption pseudocapacitance.

1. Introduction

Supercapacitors are one of the most promising energy storage technologies for applications in the fields of electric vehicles as well as miniaturization of consumer electronics, due to their high power density, long cycle life, and relatively low cost [1–3]. Two-dimensional (2D) materials such as graphene, graphene oxide, and transition metal dichalcogenides (TMDCs) are ideal materials to form supercapacitor electrodes due to their high specific surface area, conductivity and redox active structures [1,4,5]. Layered 2D materials can be produced by several techniques including; mechanical peeling [6], chemical vapor deposition (CVD) [6,7], and ultrasonic treatment in specially chosen solvents [8]. While the materials created by both mechanical peeling and CVD are of high quality and large crystal size, these production methods lack scalability and remain high cost. However, solution exfoliation can currently produce large volumes of dispersed monolayer and few layer flakes of various 2D materials, cheaply and with the potential for scale-up. These dispersions can then be deposited onto a suitable substrate or directly formed into electrodes for energy storage devices.

There have been a large number of reviews in the scientific literature that cover the application of graphene based materials for electrochemical energy storage [9–12], and their popularity has led to an increased interest in similarly structured materials, as well as composites consisting of both [1,2,5]. Despite being widely studied during the 1970s for energy storage applications as lithium ion battery electrodes, it is only more recently that nanostructures of TMDCs with reduced dimensionality have been studied and new properties discovered [2]. The varied electronic structure that TMDCs possess, ranging from insulating (HfS_2), semi-conducting (MoS_2, WS_2), to semi-metals (VS_2, TiS_2), and superconductors ($TaSe_2$, $NbSe_2$), makes them ideal for electrochemical energy storage applications [13,14]. By far the most frequently studied of these 2D TMDCs for energy storage is the semiconducting molybdenum disulphide (MoS_2 [15–18]), with several other 2D TMDCs being either unstudied, or scarcely studied, in the context of previous literature on electrochemical energy storage. Additionally, despite the popularity of research into the energy storage properties of these novel 2D materials there are very few studies that directly compare the performance of differing materials under identical conditions, allowing for a comparison of relative performance.

* Corresponding authors.
E-mail addresses: Mark.Bissett@manchester.ac.uk (M.A. Bissett), Robert.Dryfe@manchester.ac.uk (R.A.W. Dryfe).

http://dx.doi.org/10.1016/j.electacta.2016.03.190

The predominant charge storage mechanism in these TMDC cells is also unclear, with some exhibiting typical electric double layer capacitor (EDLC) responses, while others exhibit pseudocapacitance attributed to significant Faradaic charge transfer [19,20]. The individual performance of an electrode material also depends strongly on a wide variety of experimental conditions, including the electrolyte with which it is tested, as well as the cell configuration (2 electrode or 3 electrode), and the addition of any polymeric binders and conductive additives (e.g. carbon black) [21]. The popularity of conductive additives makes understanding the fundamental electrochemical performance of the individual components difficult, as although the performance is enhanced through the use of such additives, it is difficult to determine the contribution to the performance from each component. This wide degree of variation in the literature also makes it difficult to easily compare similar 2D TMDC materials for use as electrochemical energy storage electrodes and optimise them for future use in applications.

In this work we prepare solvent-stabilised dispersions of a variety of 2D layered TMDCs (MoS_2, WS_2, TiS_2, and $MoSe_2$) via ultrasonication. These dispersions are then used to create supercapacitor electrodes without the use of additives, such as conductive carbon black or polymeric binders. After characterisation of the exfoliated materials, supercapacitor electrodes were assembled into a symmetrical coin-cell type architecture and tested using an aqueous electrolyte (1 M Na_2SO_4), to allow for a direct comparison of the electrochemical energy storage behaviour for these different TMDCs under identical testing conditions. It was found that despite the overwhelming popularity in the literature of MoS_2 as an electrode material for use in supercapacitors, other TMDC materials exhibited superior charge storage behaviour. Titanium disulphide (TiS_2) displayed the best performance due to a combination of high conductivity, low density, and its intrinsic charge storage ability.

2. Experimental

2.1. Preparation of TMDC Membrane Electrodes

TMDC dispersions were created by liquid phase exfoliation as has been reported previously [22–24]. Briefly, commercially available TMDC powders (MoS_2, WS_2, TiS_2, and $MoSe_2$) were dispersed in N-methyl-2-pyrrolidone (NMP) at a concentration of 10 mg/ml and ultrasonically processed in a bath sonicator (Elmasonic P70H) operating at 37 kHz and 40% amplitude for 12 hours, while cooling to maintain a stable temperature of 20 °C. After this sonication, the dispersions were centrifuged at 6000 rpm (3139 g) for 30 minutes to remove any unexfoliated material. The supernatant was then decanted and fresh solvent (NMP) added before repeating the centrifugation at 6000 rpm to ensure removal of any unexfoliated material. The resultant suspensions were stable in solution for several months with no detectable sedimentation.

Electrodes of the exfoliated TMDCs were synthesized by first diluting the NMP dispersions in isopropanol (IPA) by a factor of 20 followed by filtering through pre-weighed polyvinylidene fluoride (PVDF) filters with 0.1 μm pore diameter. These were then washed with IPA to reduce any NMP residue and dried in an oven at 80 °C to remove any residual solvent. The TMDC membranes were then each analyzed by Raman spectroscopy, X-ray diffraction, scanning electron microscopy, and electrochemistry.

2.2. Characterisation of Exfoliated TMDC Membranes

Each of the TMDC dispersions were deposited onto a Si/SiO_2 (300 nm thickness of oxide) wafer and the solvent removed by heating on a hot plate allowing individual flakes to be identified by optical microscopy and analyzed with Raman spectroscopy. Confocal Raman spectroscopy was conducted using a Renishaw inVia microscope with a 532 nm (2.33 eV) excitation at a power of ~1 mW with a 100× objective, and a grating of 1800 l/mm to achieve a spectral resolution of ~1 cm^{-1}.

Powder X-ray diffraction (PXRD) patterns of the TMDCs, both in their bulk form and after exfoliation and filtration to form electrodes, were obtained using a PANalytical X'Pert X-ray diffractometer. Using a Cu-Kα radiation source operating at 40 kV and 30 mA the patterns were recorded whilst spinning in the range 2θ = 5–35, with a step size of 0.017 and a scan step time of 66 s. The position of the (002) peak was used to calculate the d-spacing's of the materials according to Bragg's law:

$$d = \frac{\lambda}{2sin\theta}$$

where λ is the wavelength of the radiation source (0.15418 nm) and θ is half the position of the (002) peak.

The morphology of the electrodes, as well as individual crystal flake size of the TMDC materials, were characterised using a FEI Quanta 200 scanning electron microscope (SEM). All images were obtained at 20 kV, under high vacuum utilising secondary electron detection.

2.3. Electrochemical testing of Coin Cell Supercapacitors

Cyclic voltammetry (CV) and electrochemical impedance spectroscopy (EIS) were performed using a PGSTAT302N potentiostat (Metrohm Autolab, The Netherlands). All electrochemical measurements were performed using a sealed symmetrical coin cell (CR2032). The membranes were stacked back-to-back within the coin cell with the active material making direct contact with the current collector as demonstrated previously [18,25]. The electrolyte used for all cells was aqueous Na_2SO_4 (1 M). Cyclic voltammetry was performed at scan rates ranging from 10–1000 mV/s. EIS was performed at a frequency range of 0.1 Hz to 100 kHz with a 10 mV (RMS) perturbation and 0 V dc bias.

3. Results and discussion

3.1. Characterization of exfoliated TMDCs

Fig. 1a shows the crystal structures of each of the TMDCs used in this study (MoS_2, WS_2, TiS_2, $MoSe_2$), and the structural similarities can clearly be seen. Each consists of layers of 3 atoms, with the transition metal in the centre and the covalently bound chalcogen (sulphur or selenium) atoms on either side. After ultrasonication-assisted exfoliation using NMP and centrifugation to remove unexfoliated flakes, each of these materials exist as predominantly few layered (1-3) dispersions, as seen previously in literature [23,24]. The few-layered nature of these dispersions can be seen in the high stability of the dispersions, a photograph of the dispersions can be seen in Fig. 1b, with no detectable aggregation or sedimentation over extended periods of time (several months). This few-layered nature was also supported by both the UV–vis absorbance and Raman spectroscopy, as discussed below.

3.1.1. Absorption Spectroscopy

The individual UV–vis absorbance behaviour of each of the dispersions can be seen in Fig. 2. As already noted the TMDC dispersions, after ultrasonication and centrifugation to remove any unexfoliated material, remained stable for extended periods of time due to the close match in surface energy of the chosen solvent and the TMDCs themselves [24]. Although each of the different

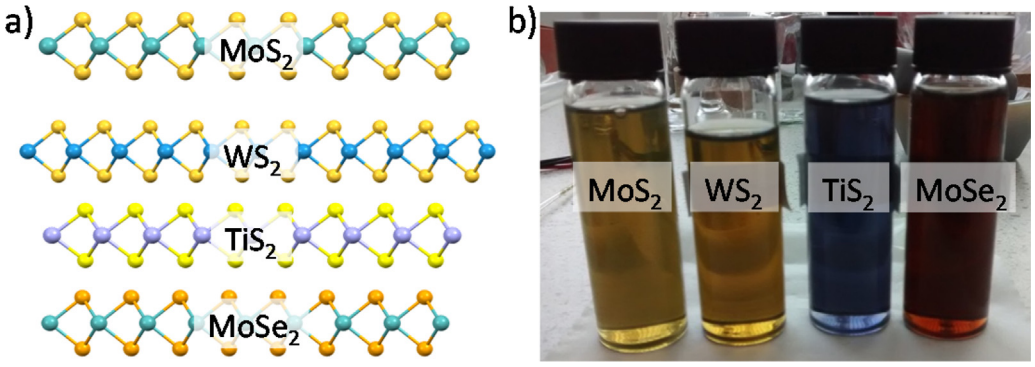

Fig. 1. Crystal structure of each of the studied 2D TMDCs in this work showing the expected 2H phase (a). Photograph of the stable TMDC dispersions (as labelled) in NMP after ultrasonication and centrifugation (b).

TMDCs studied in this work have slightly different surface energies it has been shown that certain solvents, including NMP, are able to maintain stable dispersions for each of them [22]. Due to the semiconducting nature of the TMDCs studied here (MoS_2, WS_2, and $MoSe_2$) there are distinct excitonic absorbance peaks in the spectrum corresponding to the transitions between the energy levels within the exfoliated crystals. The measured transitions from Fig. 2 are as follows; 1.98 and 2.35 eV for WS_2, 1.85 and 2.0 eV for MoS_2, 1.53 and 1.75 eV for $MoSe_2$, which match the expected transitions from the literature [22,26]. In the case of TiS_2, as it is a semi-metal it does not have an excitonic absorption, but instead a broad absorbance peak centred around 2.0 eV, assigned to the interband transition from below the Fermi level to the band in the Σ M direction [27,28].

3.1.2. Raman Spectroscopy

To further characterise the properties of the individual flakes the dispersions were diluted with IPA before being drop cast onto silicon wafers, with a 300 nm thick SiO_2 layer, for Raman analysis. This dilution allows discrete flakes to be observed and minimises the restacking of flakes that occurs as the solvent evaporates. Thin flakes could then be optically detected due to the change in optical contrast [29]. Raman spectroscopy is an ideal tool to quickly and non-destructively characterise the exfoliated 2D crystals, as it provides information regarding both the electronic and physical structure of the material including; the thickness of the flakes, the presence of defects, and also the presence of any doping or strain [30–32]. The most relevant Raman active vibration in the 2D materials studied in this work is the out-of-plane A_{1g} vibration, as this is strongly affected by neighbouring layers and can be used to indicate that exfoliation has occurred successfully.

In Fig. 3 the most intense Raman peaks have been labelled for each of the investigated materials. For each material the Raman analysis indicates that the solution exfoliated flakes consist of a mix of few-layer flakes, consisting of 1-3 layers [32]. For MoS_2 the main peaks are the in-plane E^1_{2g} (382.7 cm^{-1}) and the out-of-plane A_{1g} (407.3 cm^{-1}), consistent with a thickness of few-layer (1-3) flakes [24]. The Raman spectrum of the WS_2 also matches the previous literature reports for few layer flakes, with the A_{1g} (416.7 cm^{-1}) as well as the overlapping 2LA and E^1_{2g} peaks both labelled [33]. The exfoliated TiS_2 has a broad A_{1g} peak (329.4 cm^{-1}) with a shoulder at 380 cm^{-1}, and a low intensity E_g peak (229.6 cm^{-1}) [34]. The $MoSe_2$ has a single high intensity A_{1g} peak which occurs at 239.3 cm^{-1}, this again indicates the formation of few-layer flakes [35,36]. As well as information regarding the thickness of the flakes, the absence of any defect-induced peaks confirms that minimal defects have been induced into the exfoliated crystals during the exfoliation process [30]. These results indicate the high quality of the exfoliated material and the suitability of solution exfoliation for large scale electrode production.

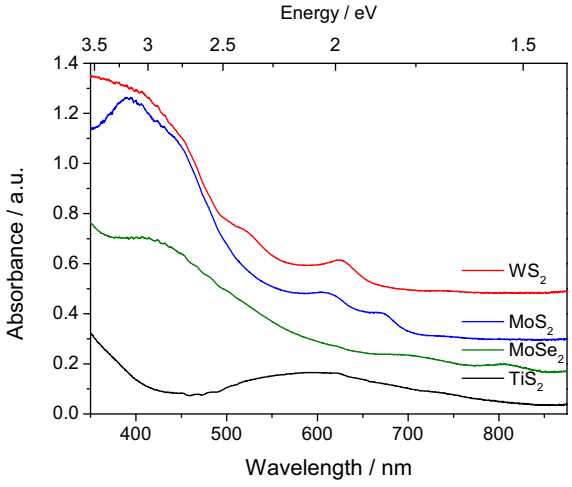

Fig. 2. UV–vis absorption spectra for each of the TMDC dispersions in NMP (as labelled). Spectra are offset vertically for clarity.

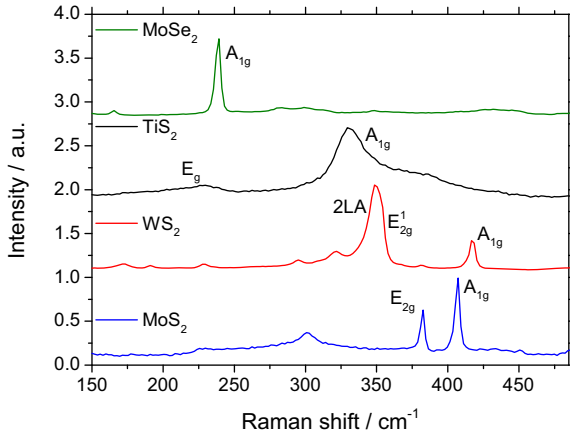

Fig. 3. Raman spectra (532 nm/2.33 eV excitation) of each of the exfoliated TMDC flakes (as labelled) after dilution and deposition onto a Si/SiO_2 wafer. The most intense Raman active vibrations (Out-of-plane A_{1g}, and in-plane E_{2g}) are labelled according to literature assignments. Spectra are offset vertically for clarity.

3.1.3. X-ray Diffraction

Supercapacitor electrodes were created by filtering the solvent-stabilised dispersions of each TMDC through PVDF membranes, without the use of any additional additives, and these supported electrodes were then analysed by X-ray diffraction to investigate any change in crystal structure. PXRD patterns of the four TMDCs as bulk materials, as well as after exfoliation and formation into electrodes, are shown in Fig. 4. The positions of the (002) peaks, the corresponding calculated d-spacings, and the literature d-spacings for the same materials are each summarised in Table 1.

For each of the TMDCs the calculated d-spacing after exfoliation and filtration is slightly higher than that for the bulk materials, it is also apparent that the peaks are significantly broader. This increased layer spacing can be explained by the fact that during filtration of the dispersions and subsequent restacking of the layered materials, there will likely be stacking misorientations which would lead to a slight increase in average layer spacing. There is also the possibility of residual solvent trapped between layers which may affect the interlayer spacing. The significant increase of the peak width indicates that the crystal domains have decreased in size after exfoliation, this is to be expected as the ultrasonication process reduces the size of the bulk starting material from flakes that are several μm in diameter down to several hundreds of nm. In addition all of the calculated d-spacings compare well with literature values, further confirming the identity of the materials.

3.1.4. Scanning Electron Microscopy

To investigate the morphology of the TMDC films after filtration, as well as to verify the individual flake size, SEM analysis was performed on each of the membranes. Typical SEM images of each of the four TMDC electrodes are shown in Fig. 5. The membranes were deliberately cut so that the cross section of the active material (TMDC) could be seen with respect to the underlying supporting membrane (PVDF). Each of the images shows that the morphology of the material on the membrane is similar, with the exfoliated flakes restacking horizontally into a 'paper' like structure. The images also indicate that the thicknesses of the TMDC coatings on the membranes vary from around 0.5 μm to 1 μm, and that the flake size is on the order of a few hundred nm. This is in agreement with previous work using similar exfoliation and centrifugation parameters [23,24].

3.2. Electrochemistry of TMDCs Electrodes

3.2.1. Cyclic Voltammetry

For electrochemical testing the membranes formed from the filtration of the TMDC dispersions were used without further modification. A photograph of one such membrane (MoS_2) can be seen in Fig. 6b. The mass of the active material was ~1 mg and from our previous study on similar membranes the average thickness of the active material layer is ~0.5 μm [18]. This is in agreement with the SEM results discussed previously. These membranes were stacked back-to-back inside a symmetrical sealed coin cell architecture (CR2032), one such assembled cell is shown in Fig. 6c, where the supporting PVDF membrane itself acts as the ion porous separator and the active material is directly in contact with

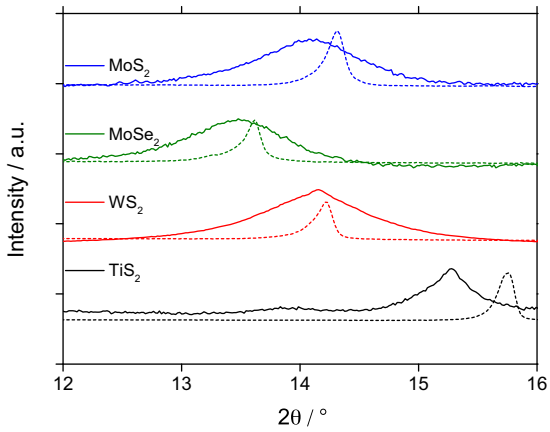

Fig. 4. PXRD of the (002) peak position for the four different TMDCs (as labelled) as bulk materials (dashed line) and after exfoliation and formation into electrodes (solid line). Only the data in the range 2θ = 12–16 is displayed in order to exclude peaks from the supporting membrane.

the current collector. This back-to-back cell architecture has been demonstrated previously and allows for simple comparison of different electrode materials without any binding polymers or conductive additives [16,18,25,41]. The electrolyte used for all the cells in this work was an aqueous solution of 1 M Na_2SO_4. The use of a pH neutral electrolyte, as opposed to strong acids or alkaline solutions, is to avoid unwanted side-reactions such as hydrogen evolution and oxygen reduction that can occur due to the highly catalytic nature of the TMDC materials, thus obscuring the fundamental capacitive behaviour [5,42,43].

Fig. 6a shows the cyclic voltammogram of each of the TMDC membranes assembled into symmetrical coin cells, at a scan rate of 50 mV/s. Each of the cells approximately exhibits the expected 'square' shape for electric double layer charge storage. This indicates that redox reactions contribute very little to the measured current for any of the studied materials over the potential range investigated (1 V), contrary to some reports which state that the predominant charge storage mechanism in similar systems is Faradaic, due to change of the transition metal oxidation state. The differing performance of each exfoliated film can be attributed to differences in conductivity, different specific surface area of the materials due to their differing densities (currents are normalised by mass of active material), and the differing intrinsic charge storage ability of each material.

From the results in Fig. 6a we see that the $MoSe_2$ film exhibits the lowest gravimetric capacitance, followed by MoS_2, then the WS_2, finally the TiS_2 electrodes displayed the highest capacitance. As mentioned this can be partially attributed to the low density of bulk TiS_2 (3.22 g/cm^3) compared to the other materials ($MoSe_2$: 6.98, WS_2: 7.5, MoS_2: 5.06 g/cm^3). The exfoliated layers that restack to form the active material of the membrane will possibly have a lower density due to imperfect stacking, however the trend of density will remain similar. However, as well as the differing densities there is a significant difference in electronic structure. As discussed TiS_2 is a semi-metal, meaning that it has a much higher

Table 1
(002) Peak positions and corresponding calculated d-spacing's for each of the TMDC materials. Literature d-spacing values are also shown.

TMDC	Bulk (002) peak position 2θ/°	Electrode (002) peak position 2θ/°	Bulk Calculated d-spacing/Å	Electrode Calculated d-spacing/Å	Literature d-spacing/Å
MoS_2	14.319	14.112	6.19	6.27	6.15 [37]
$MoSe_2$	13.621	13.498	6.50	6.55	6.45 [38]
WS_2	14.222	14.169	6.22	6.25	6.20 [39]
TiS_2	15.753	15.279	5.62	5.79	5.72 [40]

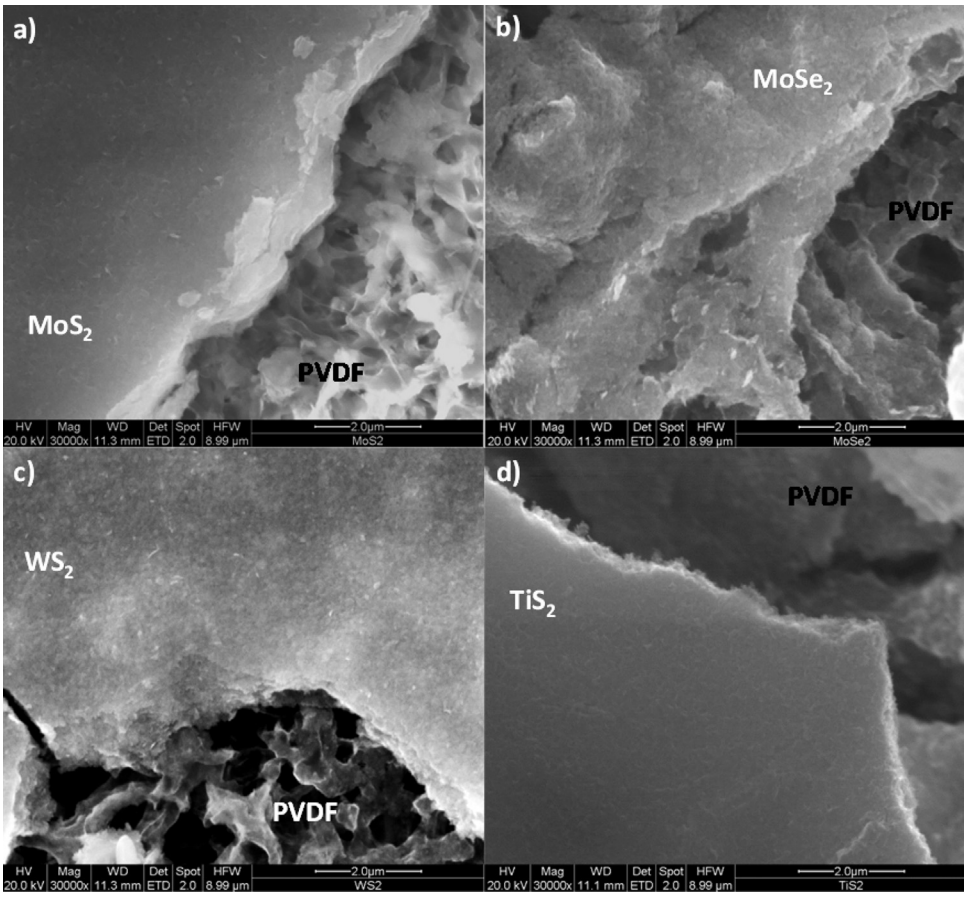

Fig. 5. Scanning Electron Micrographs of each of the TMDC membranes; MoS_2 (a), $MoSe_2$ (b), WS_2 (c), and TiS_2 (d), supported on PVDF filters (as labelled). The scale bar for each image is 2 μm.

conductivity than the other materials studied and this allows it to store charge much more efficiently by avoiding resistive losses. The reported resistivities for the bulk form of the studied materials are similar for the three semi-conductors; 10 Ω cm for MoS_2, ~10 Ω cm for WS_2, and 1.5 Ω cm for $MoSe_2$ [26,44]. This then decreases dramatically by several orders of magnitude to 5×10^{-3} Ω cm for the semi-metallic TiS_2 [26]. As well as the advantage of low density and high conductivity the intrinsic charge storage properties for different TMDCs can vary dramatically due to the differing electronic structure that arises from the interaction between the metal atom and the bound chalcogen [45]. In previous theoretical work it was predicted that TiS_2 would make an ideal pseudocapacitor electrode due to its unoccupied d-orbitals. This was also shown experimentally for TiS_2 nanocrystals when used for lithium intercalation pseudocapacitor electrodes in an organic electrolyte [46]. In this previous work a high intercalation pseudocapacitive current was measured at very low scan rates (1 mV/s) with no detectable phase shift or volume expansion when cycled.

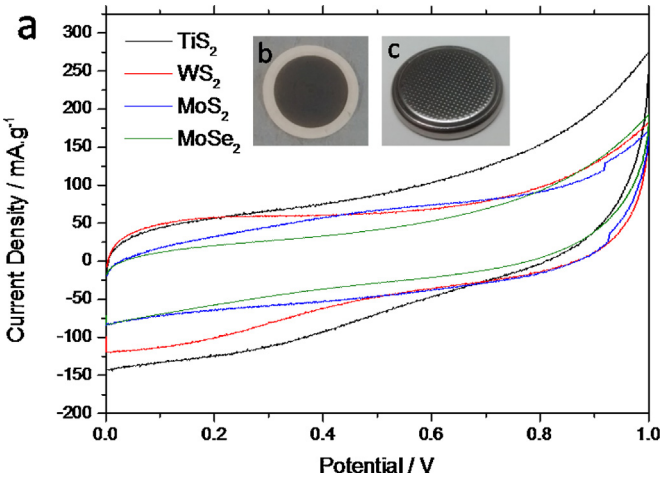

Fig. 6. Cyclic voltammograms of symmetrical coin cells for each of the TMDC electrodes. The scan rate is 50 mV/s and the electrolyte is aqueous 1 M Na_2SO_4 (a). Photograph of a typical PVDF supported TMDC membrane (MoS_2) used as the electrodes in the coin cells (b). Photograph of one such sealed coin cell (CR2032) (c).

The gravimetric specific capacitances from the TMDC based coin cells described here, calculated using cyclic voltammetry at a scan rate of 10 mV/s, are 2.57 F/g ($MoSe_2$), 3.40 F/g (MoS_2), 3.50 F/g (WS_2), and 4.60 F/g (TiS_2). These values are lower than those occasionally reported in the literature for such TMDC systems, as highly conductive and large surface area additives are added, yet the mass of these additives is often excluded from the calculation of the gravimetric specific capacitance. Although for similar additive free TMDC systems a similar range of specific capacitances is often quoted from 2–3 F/g up to 40 F/g, depending on the measurement conditions [43,47]. The cyclic voltammograms for each of the studied TMDC devices at a range of scan rates is shown in the supplementary material (Fig. S1).

It is worth noting that typically TiS_2 spontaneously reacts with water, even under atmospheric exposure, to rapidly form TiO_2 (giving off H_2S as an easily detected by-product). This would lead to the formation of a relatively insulating material, with reduced

capacitive activity, and this transformation is known to occur preferentially along the nanosheets edges [48,49]. However, this was not observed in our procedure, with no detectable change in the conductivity of the electrodes after being exposed to the aqueous electrolyte solution over time. The Raman spectrum of the solution exfoliated TiS_2, seen previously in Fig. 3, is also distinctly different from that of TiO_2 [50], which indicates that despite atmospheric exposure and exposure to laser irradiation that no oxidation occurs. The reason for this may be a residual protective layer of NMP molecules formed during the exfoliation procedure. It has been shown previously that despite repeated washing, or exposure to high temperature vacuum annealing, residual NMP molecules form a layer on the surface of solution phase exfoliated 2D materials (~11 wt% for graphene) [51]. The protective ability of this residual solvent layer has even been shown recently to protect against oxidation for highly reactive exfoliated nanosheets of black phosphorous [52,53], and we propose a similar protective mechanism occurs in the present procedure. Undoubtedly some oxidation will occur at edges and defect sites on the exfoliated TiS_2 sheets, but the extent of this transformation is reduced by the protective residual solvent. Studies on the chemical activity of the partially oxidised TiS_2-TiO_2 heterostructures that form due to the partial oxidation of exfoliated TiS_2 nanosheets have indicated that they may have unique catalytic properties and a tuneable band gap, and these warrant further investigation [49].

3.2.2. Electrochemical Impedance Spectroscopy

To investigate the frequency response of the capacitor devices electrochemical impedance spectroscopy (EIS) was performed. In the case of an ideal EDLC the phase angle between the real and complex components of the impedance should be 90° across all frequencies. However, real supercapacitors typically alternate between behaving as an ideal resistor at high frequency and an ideal capacitor at low frequency, while at the intermediate frequencies the impedance response resembles a combination of both resistance and capacitance [54]. Fig. 7 plots the phase angle as a function of frequency for each of the different supercapacitor coin cells (Bode plot). As expected each of the materials displays a high phase angle at low frequency (0.1 Hz) where the cell is in the ideal capacitor region which then decreases at high frequency (100 kHz) as resistance becomes dominant. However, we also see distinct differences between the impedance responses of each of the materials. This is due to the intrinsic differences in the electronic structure and the charge storage mechanisms that occur in each material. The MoS_2 cell exhibits the lowest phase angle at low frequency (60°) and this remains approximately constant until 1 kHz where it drops to a minimum. The WS_2 cell displays similar behaviour, starting initially at ~75° and reducing slightly up until

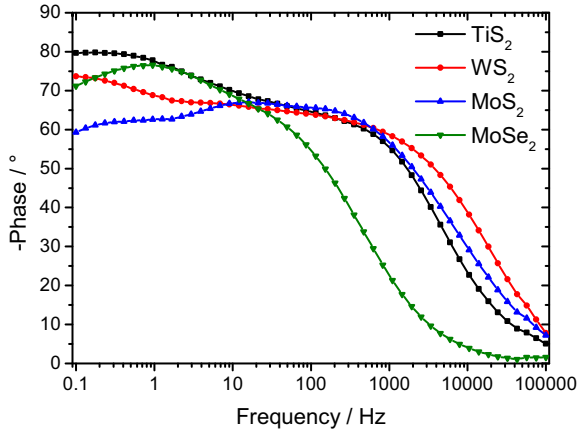

Fig. 7. Plot of phase angle against frequency (Bode plot) for each of the assembled coin cells.

~2 kHz when it drops rapidly. The phase of the $MoSe_2$ cell decreases at a much lower frequency (~100 Hz) than the other cells, this indicates that the transition to the resistive regime begins at a much lower time constant. The TiS_2 however, again displays excellent capacitive behaviour, with the phase at low frequency as high as 80° and again switching to the resistive regime at ~1 kHz. This indicates the high rate capability of the TiS_2 electrode for both charging and discharging compared to the other similar materials.

To better understand the behavior of the TMDC membranes at a range of frequencies we can also calculate the capacitance as a function of frequency, and this consists of both the real ($C_{(\omega)}$) and complex ($C''_{(\omega)}$) components using equations (1) and (2) [54]. The low frequency values of C' corresponds to the capacitance of the system during discharge, while C'' corresponds to the irreversible energy losses.

$$C'_{(\omega)} = \frac{-Z''_{(\omega)}}{\omega |Z_{(\omega)}|^2} \quad (1)$$

$$C''_{(\omega)} = \frac{Z'_{(\omega)}}{\omega |Z_{(\omega)}|^2} \quad (2)$$

The normalised real and complex capacitances as a function of frequency are plotted for each of the analysed cells in Fig. 8. In Fig. 8a we can see that, as the frequency is increased, the real

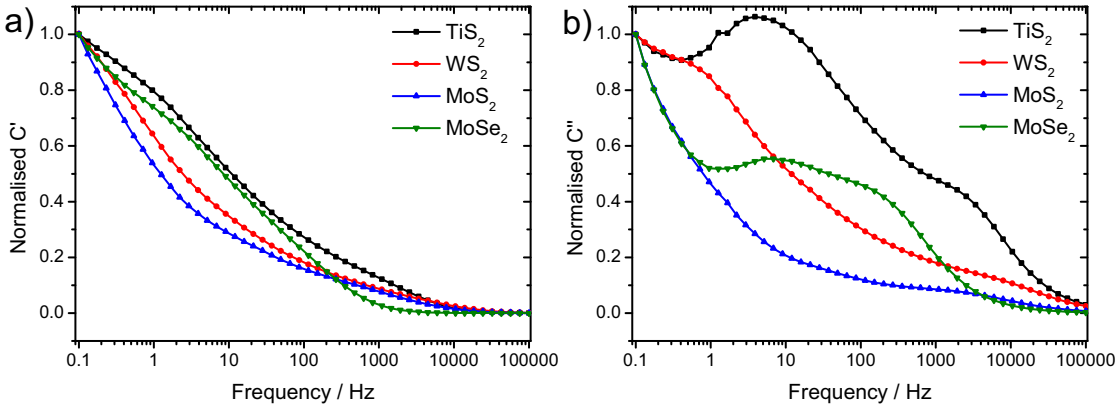

Fig. 8. Normalised (C/C_0) plot of real capacitance (C') (a) and complex capacitance (C'') (b) against frequency for each of the assembled coin cells as labelled.

component of the capacitance decreases as expected, and the slope of this decrease is characteristic of the electrode/electrolyte interface for each membrane [54]. We also see in Fig. 8a that the TiS_2 membrane exhibits superior capacitive behaviour across the range of frequencies, while the MoS_2 membrane suffers from the largest decrease in capacitance (C′) with increasing frequency. This matches what has been seen previously for very thin layers of TMDCs [55].

Fig. 8b plots the normalised complex component of the capacitance (C″) as a function of frequency. From Equation (2) we expect C″ to go through a maximum at a specific frequency, which is defined as the dielectric relaxation time for the system [54]. This time constant represents the rate at which the system can be discharged, with the system dominated by resistive behaviour at frequencies above this constant and an ideal capacitor at frequencies below it. From Fig. 8b the TiS_2 membrane appears to have two peaks in the plot of C″, indicating that another charge storage mechanism, beyond pure EDLC, must be occurring. From a wide variety of previous works on TMDC based pseudocapacitors this second charge storage can be attributed to electrolyte ion adsorption-based pseudocapacitance [18,45,46]. The time constant for the TiS_2 peaks corresponds firstly to 0.52 ms which is most likely for the rapid EDLC charge storage, and 0.26 s for the slower but much larger magnitude pseudocapacitance. The WS_2 membrane also exhibits two separated peaks, with time constants of 0.22 ms and 1.4 s, while for the $MoSe_2$ membrane they overlap more closely at 6.0 ms and 0.08 s. The MoS_2 membrane only exhibits a single very low intensity peak at the high frequency end of the plot, indicating that only a limited amount of EDLC charge storage occurs, the time constant for this peak is similar to the other materials at 0.6 ms. This also indicates that for the MoS_2 the ion adsorption occurs on very slow timescale when compared to the other TMDCs, as it is below the range of frequencies studied. This is supported by a wide variety of previous publications on the capacitive performance of MoS_2 based membranes which showed exceptionally high specific capacitances for very low scan rates (low current densities), which then suffered from rapid decreases in performance compared to purely EDLC based devices as the charge or discharge speed was increased [16–18,55,56]. From these results we can see that for each of the studied 2D exfoliated TMDC membranes that two distinct charge storage mechanisms occur on different timescales, with both the low magnitude but rapid EDLC behaviour combined with the much larger magnitude but much slower ion adsorption pseudocapacitance. These results, which show distinctly different electrochemical processes are occurring in each cell, are in agreement with similar theoretical studies on the different charge storage mechanisms of TMDC materials [45,57].

The dual operation of these charge storage mechanisms, which occur on different time scales, is important when considering for the transfer of these TMDC-based supercapacitors into real world applications. The beneficial performance measured previously in composites of these TMDC materials for use in supercapacitor devices has been achieved by combining high conductivity and high surface area materials, which inherently possess higher EDLC charge storage capabilities, with the excellent ion adsorption properties of the TMDC crystals and this allows us to further optimise these systems going forward [18,25].

4. Conclusions

In this work we have demonstrated that despite being the most widely studied layered TMDC material in previous literature, the charge storage properties of MoS_2 are in fact inferior to many analogous materials such as WS_2 or $MoSe_2$ due to the differences in charge storage mechanism of each material. The higher intrinsic charge storage ability, combined with the higher conductivity and lower density of TiS_2, exhibited increased specific capacitance, approximately twice that of the MoS_2. This capacitive performance was possible using an aqueous electrolyte, where the residual NMP molecules from the exfoliation procedure formed a protective layer and thereby protected the TiS_2 from oxidation to TiO_2. This demonstrates that it should be possible to perform aqueous electrochemistry on a variety of 2D materials previously regarded as unstable. By analysing the frequency response of each of the TMDC coin cells it was possible to differentiate between the differing charge storage mechanisms underway, which are found to be in agreement with previous theoretical predictions. It was found that each cell exhibited a rapid, but comparatively low magnitude, double-layer response. At slower rates the much larger magnitude ion adsorption pseudocapacitance was the dominant charge storage mechanism. This finding of temporally distinct charge storage regimes is important for designing future devices on exfoliated TMDC materials.

Acknowledgments

The authors wish to acknowledge funding from the EPSRC (grant ref. EP/K016954/1).

Appendix A. Supplementary data

Supplementary data associated with this article can be found, in the online version, at http://dx.doi.org/10.1016/j.electacta.2016.03.190.

References

[1] H. Wang, H. Feng, J. Li, Graphene and graphene-like layered transition metal dichalcogenides in energy conversion and storage, Small 10 (2014) 2165–2181.
[2] Z. Yu, L. Tetard, L. Zhai, J. Thomas, Supercapacitor electrode materials: nanostructures from 0 to 3 dimensions, Energy Environ. Sci. 8 (2015) 702–730.
[3] P. Simon, Y. Gogotsi, Materials for electrochemical capacitors, Nat. Mater. 7 (2008) 845–854.
[4] M.-R. Gao, Y.-F. Xu, J. Jiang, S.-H. Yu, Nanostructured metal chalcogenides: synthesis, modification, and applications in energy conversion and storage devices, Chem. Soc. Rev. 42 (2013) 2986–3017.
[5] C.N.R. Rao, K. Gopalakrishnan, U. Maitra, Comparative study of potential applications of graphene, MoS_2, and other two-dimensional materials in energy devices, sensors, and related areas, ACS Appl. Mater. Interfaces 7 (2015) 7809–7832.
[6] K.S. Novoselov, D. Jiang, F. Schedin, T.J. Booth, V.V. Khotkevich, S.V. Morozov, A. K. Geim, Two-dimensional atomic crystals, Proc. Natl. Acad. Sci. U.S.A. 102 (2005) 10451–10453.
[7] Y. Zhang, L. Zhang, C. Zhou, Review of chemical vapor deposition of graphene and related applications, Acc. Chem. Res. 46 (2013) 2329–2339.
[8] V. Nicolosi, M. Chhowalla, M.G. Kanatzidis, M.S. Strano, J.N. Coleman, Liquid exfoliation of layered materials, Science 340 (2013) 1226419.
[9] R. Raccichini, A. Varzi, S. Passerini, B. Scrosati, The role of graphene for electrochemical energy storage, Nat. Mater. 14 (2015) 271–279.
[10] Y. Huang, J. Liang, Y. Chen, An overview of the applications of graphene-based materials in supercapacitors, Small 8 (2012) 1805–1834.
[11] J. Chen, C. Li, G. Shi, Graphene materials for electrochemical capacitors, J. Phys. Chem. Lett. 4 (2013) 1244–1253.
[12] G. Xiong, C. Meng, R.G. Reifenberger, P.P. Irazoqui, T.S. Fisher, A review of graphene-based electrochemical microsupercapacitors, Electroanalysis 26 (2014) 30–51.
[13] Q.H. Wang, K. Kalantar-Zadeh, A. Kis, J.N. Coleman, M.S. Strano, Electronics and optoelectronics of two-dimensional transition metal dichalcogenides, Nat. Nanotechnol. 7 (2012) 699–712.
[14] M. Chhowalla, H.S. Shin, G. Eda, L.-J. Li, K.P. Loh, H. Zhang, The chemistry of two-dimensional layered transition metal dichalcogenide nanosheets, Nat. Chem. 5 (2013) 263–275.
[15] L. Cao, S. Yang, W. Gao, Z. Liu, Y. Gong, L. Ma, G. Shi, S. Lei, Y. Zhang, S. Zhang, R. Vajtai, P.M. Ajayan, Direct laser-patterned micro-supercapacitors from paintable MoS_2 films, Small 9 (2013) 2905–2910.
[16] A. Winchester, S. Ghosh, S. Feng, A.L. Elias, T. Mallouk, M. Terrones, S. Talapatra, Electrochemical characterization of liquid phase exfoliated two-dimensional layers of molybdenum disulfide, ACS Appl. Mater. Interfaces 6 (2014) 2125–2130.
[17] M. Acerce, D. Voiry, M. Chhowalla, Metallic 1T phase MoS_2 nanosheets as supercapacitor electrode materials, Nat. Nanotechnol. 10 (2015) 313–318.

[18] M.A. Bissett, I.A. Kinloch, R.A.W. Dryfe, Characterization of MoS_2-graphene composites for high-performance coin cell supercapacitors, ACS Appl. Mater. Interfaces 7 (2015) 17388–17398.
[19] B.E. Conway, V. Birss, J. Wojtowicz, The role and utilization of pseudocapacitance for energy storage by supercapacitors, J. Power Sources 66 (1997) 1–14.
[20] B.E. Conway, Transition from supercapacitor to battery behavior in electrochemical energy storage, J. Electrochem. Soc. 138 (1991) 1539–1548.
[21] M.D. Stoller, R.S. Ruoff, Best practice methods for determining an electrode material's performance for ultracapacitors, Energy Environ. Sci. 3 (2010) 1294–1301.
[22] G. Cunningham, M. Lotya, C.S. Cucinotta, S. Sanvito, S.D. Bergin, R. Menzel, M.S. P. Shaffer, J.N. Coleman, Solvent exfoliation of transition metal dichalcogenides: Dispersibility of exfoliated nanosheets varies only weakly between compounds, ACS Nano 6 (2012) 3468–3480.
[23] A. O'Neill, U. Khan, J.N. Coleman, Preparation of high concentration dispersions of exfoliated MoS_2 with increased flake size, Chem. Mater. 24 (2012) 2414–2421.
[24] J.N. Coleman, M. Lotya, A. O'Neill, S.D. Bergin, P.J. King, U. Khan, K. Young, A. Gaucher, S. De, R.J. Smith, I.V. Shvets, S.K. Arora, G. Stanton, H.-Y. Kim, K. Lee, G. T. Kim, G.S. Duesberg, T. Hallam, J.J. Boland, J.J. Wang, J.F. Donegan, J.C. Grunlan, G. Moriarty, A. Shmeliov, R.J. Nicholls, J.M. Perkins, E.M. Grieveson, K. Theuwissen, D.W. McComb, P.D. Nellist, V. Nicolosi, Two-dimensional nanosheets produced by liquid exfoliation of layered materials, Science 331 (2011) 568–571.
[25] N. Savjani, E.A. Lewis, M.A. Bissett, J.R. Brent, R.A.W. Dryfe, S.J. Haigh, P. O'Brien, Synthesis of lateral size-controlled monolayer 1H-MoS_2@oleylamine as supercapacitor electrodes, Chem. Mater. 28 (2016) 657–664.
[26] J.A. Wilson, A.D. Yoffe, The transition metal dichalcogenides discussion and interpretation of the observed optical, electrical and structural properties, Adv. Phys. 18 (1969) 193–335.
[27] A.H. Reshak, S. Auluck, Electronic and optical properties of the 1T phases of TiS_2, $TiSe_2$, and $TiTe_2$, Phys. Rev. B 68 (2003) 245113.
[28] D. Rossi, J.H. Han, D. Yoo, Y. Dong, Y. Park, J. Cheon, D.H. Son, Photoinduced separation of strongly interacting 2-D layered TiS_2 nanodiscs in solution, J. Phys. Chem. C 118 (2014) 12568–12573.
[29] H. Li, J. Wu, X. Huang, G. Lu, J. Yang, X. Lu, Q. Xiong, H. Zhang, Rapid and reliable thickness identification of two-dimensional nanosheets using optical microscopy, ACS Nano 7 (2013) 10344–10353.
[30] M.A. Pimenta, E. del Corro, B.R. Carvalho, C. Fantini, L.M. Malard, Comparative study of raman spectroscopy in graphene and MoS_2-type transition metal dichalcogenides, Acc. Chem. Res. 48 (2015) 41–47.
[31] M.A. Bissett, M. Tsuji, H. Ago, Strain engineering the properties of graphene and other two-dimensional crystals, Phys. Chem. Chem. Phys. 16 (2014) 11124–11138.
[32] X. Zhang, X.-F. Qiao, W. Shi, J.-B. Wu, D.-S. Jiang, P.-H. Tan, Phonon and Raman scattering of two-dimensional transition metal dichalcogenides from monolayer, multilayer to bulk material, Chem. Soc. Rev. 44 (2015) 2757–2785.
[33] A. Berkdemir, H.R. Gutierrez, A.R. Botello-Mendez, N. Perea-Lopez, A.L. Elias, C.-I. Chia, B. Wang, V.H. Crespi, F. Lopez-Urias, J.-C. Charlier, H. Terrones, M. Terrones, Identification of individual and few layers of WS_2 using Raman spectroscopy, Sci. Rep 3 (2013) 1755.
[34] M. Ishii, M. Saeki, I. Kawada, Raman study of non-stoichiometric titanium sulfides, physica status solidi (b) 124 (1984) K109–K112.
[35] P. Tonndorf, R. Schmidt, P. Böttger, X. Zhang, J. Börner, A. Liebig, M. Albrecht, C. Kloc, O. Gordan, D.R.T. Zahn, S. Michaelis de Vasconcellos, R. Bratschitsch, Photoluminescence emission and Raman response of monolayer MoS_2, $MoSe_2$, and WSe_2, Opt. Express 21 (2013) 4908–4916.
[36] X. Lu, M.I.B. Utama, J. Lin, X. Gong, J. Zhang, Y. Zhao, S.T. Pantelides, J. Wang, Z. Dong, Z. Liu, W. Zhou, Q. Xiong, Large-area synthesis of monolayer and few-layer $MoSe_2$ films on SiO_2 substrates, Nano Lett. 14 (2014) 2419–2425.
[37] M.-R. Gao, M.K.Y. Chan, Y. Sun, Edge-terminated molybdenum disulfide with a 9.4-A interlayer spacing for electrochemical hydrogen production, Nat. Commun. 6 (2015).
[38] P.B. James, M.T. Lavik, The crystal structure of $MoSe_2$, Acta Crystallogr. 16 (1963) 1183.
[39] J. Yang, D. Voiry, S.J. Ahn, D. Kang, A.Y. Kim, M. Chhowalla, H.S. Shin, Two-dimensional hybrid nanosheets of tungsten disulfide and reduced graphene oxide as catalysts for enhanced hydrogen evolution, Angew. Chem. Int. Ed. 52 (2013) 13751–13754.
[40] J. Chen, Z.-L. Tao, S.-L. Li, Lithium intercalation in open-ended TiS_2 Nanotubes, Angew. Chem. Int. Ed. 42 (2003) 2147–2151.
[41] X. An, T. Simmons, R. Shah, C. Wolfe, K.M. Lewis, M. Washington, S.K. Nayak, S. Talapatra, S. Kar, Stable aqueous dispersions of noncovalently functionalized graphene from graphite and their multifunctional high-performance applications, Nano Lett. 10 (2010) 4295–4301.
[42] H. Wang, Z. Lu, S. Xu, D. Kong, J.J. Cha, G. Zheng, P.-C. Hsu, K. Yan, D. Bradshaw, F. B. Prinz, Y. Cui, Electrochemical tuning of vertically aligned MoS_2 nanofilms and its application in improving hydrogen evolution reaction, Proc. Natl. Acad. Sci. U.S.A. 110 (2013) 19701–19706.
[43] X. Chia, A.Y.S. Eng, A. Ambrosi, S.M. Tan, M. Pumera, Electrochemistry of nanostructured layered transition-metal dichalcogenides, Chem. Rev. 115 (2015) 11941–11966.
[44] A. Jäger-Waldau, M.C. Lux-Steiner, G. Jäger-Waldau, E. Bucher, WS_2 thin films prepared by sulphurization, Appl. Surf. Sci. 70 (1993) 731–736.
[45] X. Cong, C. Cheng, Y. Liao, Y. Ye, C. Dong, H. Sun, X. Ji, W. Zhang, P. Fang, L. Miao, J. Jiang, Intrinsic charge storage capability of transition metal dichalcogenides as pseudocapacitor electrodes, J. Phys. Chem. C 119 (2015) 20864–20870.
[46] G.A. Muller, J.B. Cook, H.-S. Kim, S.H. Tolbert, B. Dunn, High performance pseudocapacitor based on 2D layered metal chalcogenide nanocrystals, Nano Lett. 15 (2015) 1911–1917.
[47] C.C. Mayorga-Martinez, A. Ambrosi, A.Y.S. Eng, Z. Sofer, M. Pumera, Transition metal dichalcogenides (MoS_2, $MoSe_2$ WS_2 and WSe_2) exfoliation technique has strong influence upon their capacitance, Electrochem. Commun. 56 (2015) 24–28.
[48] J.H. Han, S. Lee, D. Yoo, J.-H. Lee, S. Jeong, J.-G. Kim, J. Cheon, Unveiling chemical reactivity and structural transformation of two-dimensional layered nanocrystals, J. Am. Chem. Soc. 135 (2013) 3736–3739.
[49] C.S. Cucinotta, K. Dolui, H. Pettersson, Q.M. Ramasse, E. Long, S.E. O'Brian, V. Nicolosi, S. Sanvito, Electronic properties and chemical reactivity of TiS_2 nanoflakes, J. Phys. Chem. C 119 (2015) 15707–15715.
[50] T. Ohsaka, F. Izumi, Y. Fujiki, Raman spectrum of anatase, TiO_2, J. Raman Spectrosc. 7 (1978) 321–324.
[51] Y. Hernandez, V. Nicolosi, M. Lotya, F.M. Blighe, Z. Sun, S. De, I.T. McGovern, B. Holland, M. Byrne, Y.K. Gun'Ko, J.J. Boland, P. Niraj, G. Duesberg, S. Krishnamurthy, R. Goodhue, J. Hutchison, V. Scardaci, A.C. Ferrari, J.N. Coleman, High-yield production of graphene by liquid-phase exfoliation of graphite, Nat. Nanotechnol. 3 (2008) 563–568.
[52] D. Hanlon, C. Backes, E. Doherty, C.S. Cucinotta, N.C. Berner, C. Boland, K. Lee, A. Harvey, P. Lynch, Z. Gholamvand, S. Zhang, K. Wang, G. Moynihan, A. Pokle, Q. M. Ramasse, N. McEvoy, W.J. Blau, J. Wang, G. Abellan, F. Hauke, A. Hirsch, S. Sanvito, D.D. O'Regan, G.S. Duesberg, V. Nicolosi, J.N. Coleman, Liquid exfoliation of solvent-stabilized few-layer black phosphorus for applications beyond electronics, Nat. Commun. 6 (2015) 8563.
[53] J. Kang, J.D. Wood, S.A. Wells, J.-H. Lee, X. Liu, K.-S. Chen, M.C. Hersam, Solvent exfoliation of electronic-grade, two-dimensional black phosphorus, ACS Nano 9 (2015) 3596–3604.
[54] P.L. Taberna, P. Simon, J.F. Fauvarque, Electrochemical characteristics and impedance spectroscopy studies of carbon-carbon supercapacitors, J. Electrochem. Soc. 150 (2003) A292–A300.
[55] J.M. Soon, K.P. Loh, Electrochemical double-layer capacitance of MoS_2 nanowall films electrochem, Solid-State Lett. 10 (2007) A250–A254.
[56] A. Ramadoss, T. Kim, G.-S. Kim, S.J. Kim, Enhanced activity of a hydrothermally synthesized mesoporous MoS_2 nanostructure for high performance supercapacitor applications, New J. Chem. 38 (2014) 2379–2385.
[57] X. Ji, K. Xu, C. Chen, B. Zhang, H. Wan, Y. Ruan, L. Miao, J. Jiang, Different charge-storage mechanisms in disulfide vanadium and vanadium carbide monolayer, J. Mater. Chem. A 3 (2015) 9909–9914.